HHS Public Access

Author manuscript

Cancer Lett. Author manuscript; available in PMC 2024 December 01.

Published in final edited form as:

Cancer Lett. 2023 December 01; 578: 216455. doi:10.1016/j.canlet.2023.216455.

Pancreatic Ubap2 deletion regulates glucose tolerance, inflammation, and protection from cerulein-induced pancreatitis

Ram Vinod Roy[a,b,†], **Nicolas Means**[a,b,†], **Geeta Rao**[a,b], **Sima Asfa**[a], **Venkateshwar Madka**[c], **Anindya Dey**[a,b], **Yushan Zhang**[a,b], **Monalisa Choudhury**[a,b], **Kar-Ming Fung**[b], **Danny N. Dhanasekaran**[a,d], **Jacob E. Friedman**[e], **Howard C. Crawford**[f], **Chinthalapally V. Rao**[c], **Resham Bhattacharya**[a,g], **Priyabrata Mukherjee**[a,b,*]

[a]Peggy and Charles Stephenson Cancer Center, The University of Oklahoma Health Sciences Center, Oklahoma City, Oklahoma, USA.

[b]Department of Pathology, The University of Oklahoma Health Sciences Center, Oklahoma City, Oklahoma, USA.

[c]Center for Cancer Prevention and Drug Development, Department of Medicine, Stephenson Cancer Center, University of Oklahoma Health Sciences Center, Oklahoma City, Oklahoma, USA.

[d]Department of Cell Biology, University of Oklahoma Health Science Center, Oklahoma City, OK, USA.

[e]Harold Hamm Diabetes Center, University of Oklahoma Health Sciences Center, Oklahoma City, OK, USA.

[f]Department of Surgery, Henry Ford Pancreatic Cancer Center, Henry Ford Health System, Detroit, MI, USA.

[g]Department of Obstetrics and Gynecology, University of Oklahoma Health Science Center, Oklahoma City, Oklahoma, USA.

Abstract

Ubiquitin-binding associated protein 2 (UBAP2) is reported to promote macropinocytosis and pancreatic adenocarcinoma (PDAC) growth, however, its role in normal pancreatic function remains unknown. We addressed this knowledge gap by generating UBAP2 knockout (U2KO) mice under a pancreas-specific Cre recombinase (Pdx1-Cre). Pancreatic architecture remained intact in U2KO animals, but they demonstrated slight glucose intolerance compared to controls. Upon cerulein challenge to induce pancreatitis, U2KO animals had reduced levels of several

[*]**Corresponding Author:** Priyabrata Mukherjee, 975 NE 10th Street, BRC, Room#1409a, Oklahoma City, OK, 73104, Priyabrata-Mukherjee@ouhsc.edu, phone: (405) 271-1133, fax: (405) 271-2141.
[†]Equal Contributions

Competing Interest statement: None of the authors have any conflicts of interest to disclose.

Data and materials availability: All data are available in the main text or the supplementary materials, and will be made available from Priyabrata Mukherjee.

pancreatitis-relevant cytokines, amylase and lipase in the serum, reduced tissue damage, and lessened neutrophil infiltration into the pancreatic tissue. Mechanistically, cerulein-challenged U2KO animals revealed reduced NFκB activation compared to controls. *In vitro* promoter binding studies confirmed the reduction of NF-κB binding to its target molecules supporting UBAP2 as a new regulator of inflammation in pancreatitis and may be exploited as a therapeutic target in future to inhibit pancreatitis.

Keywords

UBAP2; Glucose Intolerance; Pancreatitis; Pancreatic Ductal Adenocarcinoma

Introduction:

The pancreas has both endocrine and exocrine functions, which are used to control glucose metabolism through secretion of insulin and glucagon and digest the macromolecules consumed during a meal[1–3]. Regulation of pancreatic endocrine functions are predominated by the islets of Langerhans while exocrine functions are dominated by acinar cells [2,4,5]. To accomplish this, acinar cells have the ability to both constitutively secrete proteins and regulate exocytosis of proteins that are stored in secretory granules [6]. Dysregulation or prolonged damage to the acinar cells can result in multiple clinical disorders, including: acute pancreatitis, chronic pancreatitis, autoimmune pancreatitis, pancreatic exocrine insufficiency, and pancreatic neoplasia, some of which are considered risk factors of pancreatic ductal adenocarcinoma (PDAC) [6–9]. Notably, general pancreatitis is an inflammatory event that is considered a prerequisite and synergistic factor to *KRAS* activity and PDAC initiation [9]. PDAC is described as an exocrine tumor, one of the most aggressive forms of pancreatic cancer, and has a KRAS mutation incidence of more than 90% [10–12]. Numerous pathways are involved in PDAC pathogenesis, including: *TP53*, *SMAD*, and *KRAS* [13–15].

Previously, our group described ubiquitin-binding associated protein-2 (UBAP2) and its role in regulating PDAC growth by modulating levels of activated *KRAS* and macropinocytosis activity [16]. Using the dextran uptake assay as a read-out for macropinocytosis, Xiong *et al.,*observed a reduction in macropinocytosis levels in a panel of PDAC cell lines upon transient UBAP2 knockdown which could be mostly rescued by forced expression of an activated KRAS vector (G12V) [16]. Additionally, Xiong *et al.*, found that UBAP2 was relevant to several hallmarks of pancreatic cancer pathogenesis, from growth to metastasis [16]. Interestingly, in our description of *UBAP2* in PDAC, its expression was also found in the healthy acinar cells of the pancreas[16]. As function of UBAP2 has not been established in healthy pancreas, we now report the generation and characterization of a mouse line deleting *Ubap2* throughout the pancreatic parenchyma to address the lack of knowledge of UBAP2 function in the healthy pancreas. Additionally, we report the effects of UBAP2 on pancreatitis to elucidate relevance of UBAP2 on a pancreatic pathophysiology.

Materials and Methods:

Mouse Genotyping Polymerase Chain Reaction:

Mice were genotyped by polymerase chain reaction of tail DNA with 5′-flanking, 3′-flanking, and/or internal primers for exon 5 of *Ubap2* and exon 1 of *Pdx1*. A targeting vector carrying a *loxP*-flanked coding region of *Ubap2* (exon 5) and a puromycin/neomycin selection cassette was inserted into the wild-type *Ubap2* locus via homologous recombination. Flp recombinase-activity led to the deletion of the selection cassette resulting in a *Ubap2* floxed allele (*Ubap2*^{flox}). The PCR mix was Econotaq® PLUS GREEN 2X Master Mix (Lucigen, Middleton, WI, USA; Cat#: 30033–1) and the reaction was followed according to the manufacturer's specifications. For PCR, amplification of the target genes (*Ubap2* and *Pdx1*) was done for an initial denaturation step at 95°C for 2 min, followed by 35 cycles of denaturation at 95°C for 30s, primer annealing at 58°C for 30s, and primer extension at 72°C for 45s. Upon completion of the cycling steps, a final extension at 72°C for 5 min was given and then the reaction was stored at 4°C. The PCR products were separated on a 1 % agarose gel containing 1X GelRed® Nucleic Acid Stain (Biotium, Inc., Fremont, CA, USA; Cat#: 41003) and imaged on a UV transilluminator.

Animal Use and Euthanasia:

Animal experiments in this manuscript comply with relevant ethical regulations and protocols approved by the Institutional Animal Care and Use Committee (IACUC) at the University of Oklahoma Health Sciences Center (Protocol no: 22–071-SFCHI). When utilized, animals were euthanized through CO_2 inhalation followed by secondary euthanasia of organ collection sufficient to ensure non-recovery according to Protocol #: 22–071-SFCHI.

Blood Glucose Levels, Oral Glucose Tolerance Test, and Insulin Tolerance Test:

Non-fasting blood glucose levels were recorded prior to the experimental period. The Oral glucose tolerance test (OGTT) and insulin tolerance test (ITT) were performed in *Ubap2*$^{flox/flox}$ and U2KO mice of 3 months and 6 months of age with equal numbers of males and females per group (N=7/sex/Genotype). The ITT experiment was performed 1 week post OGTT experiments [17]. In all cases, glucose quantification was performed in blood samples obtained from the tail snip blood using the calibrated glucometer system, Contour Next EZ with Contour Next Test strips (SKU NEXT50). For OGTT, mice were fasted for 12h then received a bolus of aqueous glucose solution (1g/kg body weight) that was delivered into the stomach by a gavage probe (20-gauge, 38mm long curved, with a 2.25mm ball end) [18]. Blood glucose quantification was performed at 0 (basal), 15, 30, 60, and 120 min after the glucose load. For the ITT tests, mice were fasted for 2 hours prior to insulin administration to conform with previous literature for the optimal time [19]. Afterwards, mice were intraperitoneally injected with insulin (Sigma-Aldrich, St. Louis, MO, USA; Cat#: I9278) which was dissolved in saline and delivered at a dose of 0.75 UI/kg BW[20,21] and blood glucose levels were measured at 0, 5, 15, 30, and 60 min after the insulin load. For both, OGTT and ITT, the area under the curve (AUC) values for plasma glucose were calculated using the trapezoidal rule. Mice used to measure insulin or for subsequent molecular assays did not receive any analgesic drugs. A Mouse Ultrasensitive Insulin ELISA

kit (Alpco, Salem, NH, USA; Cat #: 80-INSMSU-E01) was used to determine insulin levels during IP-GTT timepoints of 0, 15, and 120 minutes[22].

Immunofluorescence/Immunohistochemistry:

Formalin and paraffin-fixed whole pancreas tissues were processed and paraffin-embedded by the University of Oklahoma – Health Sciences Center Histology Core Facility. Tissues were sectioned to 5μm thickness. For immunofluorescence, slides were deparaffinized with sequential incubations in xylene and ethanol. Heat-induced epitope retrieval was performed in 10mM citrate buffer or EDTA. After retrieval, slides were incubated in Dako Serum Free Protein Block (Agilent, Santa Clara, CA, USA; Cat#: X090930–2) for 30 minutes. Slides were incubated overnight at 4°C with primary antibodies (Table S1) and then incubated with secondary antibodies for 1-hour at room temperature. Coverslips were mounted with Vectashield® hardset mounting medium with DAPI (Vector Laboratories, Burlingame, CA, USA; Cat#: H-1500). Secondary antibody dilutions used for staining are as follows Insulin (1:500), glucagon (1:2000), CK-19 (1:250), amylase (1:2500), and Cpa1(1:1000).

For sirius red stain, paraffin sections were deparaffinized and rehydrated using distilled water. Following this, they were carefully immersed in a PicroSirius staining solution (Hell Bio; Cat#:HB9475) for 1 hour at room temperature. After the incubation, the slides underwent thorough washing, involving three cycles in a solution containing 0.5% glacial acetic acid. Sections were rapidly dehydrated using 100% ethanol, and finally mounted in mounting solution (Leica; Cat#:3801705). Alcian blue and Masson's Trichrome stains were performed according to the manufacturer's instructions respectively (Sigma; Cat#:1.32657.001 & Ht15-B9475). For PAS staining, stains were performed according to the manufacturer's instructions (Sigma; Cat#: 395B), To enhance the contrast and highlight cellular features, the slides were counter-stained with Hematoxylin (Abcam; Cat#: ab220365) for a brief period of 30 seconds. Finally, the sections were carefully dehydrated and securely mounted in mounting solution (Leica; Cat#:3801705).

RNA Extraction, cDNA synthesis, and RT-PCR:

Total RNA was extracted using the Quick-RNA Mini-Prep kit (Zymo Research, Irvine, CA, USA; Cat#: R1055) according to the manufacturer's instructions. 1μg of total RNA was used for I-Script Select cDNA Synthesis with random primers according to the manufacturer's instructions (Bio-Rad, Irvine, California, USA; Cat#: 170–8897). For RT-PCR, amplification of target genes (Cpa1, Glucagon, Insulin, Somstatin, Amylase, CK19) was done for an initial denaturation step at 95°C for 5 min, followed by 35 cycles of denaturation at 95°C for 30s, primer annealing at 58°C for 30s, and primer extension at 72°C for 45s. Upon completion of the cycling steps, a final extension at 72°C for 5 min was done and then the reaction was stored at 4°C. Reactions were run in triplicate in three independent experiments. The geometric mean of the housekeeping genes B2M and 18S were used as internal controls to normalize the variability in expression levels. The primer sequences are provided in Supplemental Table S2.

Cerulein-Induced Pancreatitis (AP):

Pancreatitis was induced by intraperitoneal injection of 50 μg/kg cerulein (Sigma; Cat#: C9026) in 0.05M ammonium hydroxide (NH_4OH) in phosphate buffered saline (PBS) at hourly intervals for 8 hours, as previously described [23–25]. Controls were untreated or received equal volumes of 0.05M NH_4OH/PBS injected intraperitoneally. Blood and tissue samples were collected 1 hour after the last injection, for a total of 8 hours [26].

Serum Collection and Enzymatic Amylase and Lipase Analysis:

Mice were humanely euthanized according to the specifications previously mentioned. Blood was taken at the time of organ collection through a cardiac stab, and approximately 800uL of blood was collected. Collected blood was placed in 1.5mL tubes without anticoagulants and incubated at room temperature for 1 hour. Blood was spun at 1500g for 15 minutes and the serum was collected. Amylase and lipase levels were determined through routine clinical methods and analyzed through the IDEXX Catalyst One software and clips (Idexx Laboratories, Westbrook, ME, USA; Cat#: AMYL: 98–11068-01 and LIPA: 98–11079-01). Fold changes for enzymatic secretions were calculated by (cerulein group / control group) minus 1.

Mouse Cytokine Array:

The Proteome Profiler Mouse Cytokine Array Kit, (R&D Systems, Minneapolis, MN, USA; Cat#: ARY006) was used to quantify the 40 mouse proteins (cytokines, chemokines and growth factors) from the serum of mice either given PBS or cerulein and was collected as described above. Briefly, the collected serum was pooled from 5 animals and then diluted 1:2 in buffer 6. Diluted, pooled serum was then mixed with a cocktail of biotinylated antibodies for detection. The following sample/antibody mixture was then incubated with the array membranes overnight at 4 °C while rocking gently. The membranes were washed and incubated with streptavidin–horseradish peroxidase followed by chemiluminescent detection. The array data were quantitated to generate a protein profile using HL Image++ Software (Western Image Software, L.C.). Selected molecules were then presented as a fold-change value relative to the PBS control in each treatment group. The values are determined using the raw average pixel intensity from the same membranes (two duplicate spots on the membrane). The data presented is from single pool from 5 animals/genotype/group (N_{total} = 20 samples generating 4 pooled samples).

In vitro Cell Culture:

Rat pancreatic AR42J acinar cells were purchased from ATCC (American Type Culture Collection, Manassas, Virginia, USA; Cat#:CRL1492) and maintained in F-12K (ATCC; Cat#:30–2004) medium supplemented with 20% fetal bovine serum (FBS, Corning) and 1% penicillin/streptomycin (P/S, Sigma Aldrich; Cat#: P4333). Medium was replaced every 72 hours and cells were passaged once a week. Cells were detached by means of trypsin (Caisson Labs, Smithfield, UT, USA; Cat#: TRL01). If cells were thawed from frozen stocks, they were supplemented with F-12K and 40% FBS. Cells were kept at 37°C with 5% CO_2. After thawing, cells were allowed to grow and acclimatized for 4 to 6 weeks (4 to 6 passages) prior to performing experiments.

In vitro Cerulein-Induced Pancreatitis:

Cells were seeded for experiments in 6 well plates (TPP, Sigma-Aldrich) at concentrations of 7.5×10^5 /well for transfections. Cells were transiently transfected with either a non-targeting scramble siRNA or an siRNA targeting Ubap2. After 6 hours, cells were replaced with their complete medium supplemented with 150nM Dexamethasone (Sigma-Aldrich, Cat#: D4902) for 48 hours and allowed for differentiation into an acinar-like phenotype. After dexamethasone treatment, cell medium was replaced with medium containing 150nM dexamethasone and 150nM cerulein for 24 hours. Controls had complete medium only. After harvesting, for Ubap2 knockdown was confirmed from isolated RNA using protocols mentioned previously.

Chromatin Immunoprecipitation Assay:

The MAGnify™ Chromatin Immunoprecipitation System (Thermofisher, Cat#: 492024) was purchased and used according to manufacturer's specifications. Briefly, two million AR42J cells were grown on 10 centimeter plates. Cross-linking was performed by adding formaldehyde to culture media to a final concentration of 1% for 15 mins. Cells were washed with ice-cold PBS containing protease inhibitor. Cells were pelleted by centrifugation at 3500*g* for 5 mins at 4°C. Cross-linked chromatin was sonicated to shear DNA on ice to lengths between 300 to 1000 base pairs. The sonicated samples were pre-cleaned by protein A-agarose beads. Pre-cleaned chromatin was mixed with chip grade NFKB-p65 (sc-8008X, Santa Cruz, 2 μg) antibodies and were allowed to mix and were rotated overnight at 4°C and precipitated with 20ul protein A-agarose slurry for 2 hours with rotation to collect the antibody /chromatin complex. These complexes were washed and the DNA fragments were eluted by heating 65°C for 30 minutes. These eluted DNA was analyzed by PCR amplification. For PCR, amplification of the immuno-precipitated DNA was done for an initial denaturation step at 95°C for 5 min, followed by 35 cycles of denaturation at 95°C for 30s, primer annealing at 55°C for 30s, and primer extension at 72°C for 45s. Upon completion of the cycling steps, a final extension at 72°C for 5 min was given and then the reaction was stored at 4°C. The PCR products were separated on a 1 % agarose gel containing 1X GelRed® Nucleic Acid Stain.

Results

Generation and characterization of *Ubap2* knock-out mice.

We generated a new mouse line that carries a *Ubap2* allele with exon 5 of the coding region flanked by two *loxP*-recognition sites for Cre recombinase. Cre recombinase was driven by the pancreatic specific gene *Pdx1* (*Pdx1-Cre*) [27]. The Cre enzyme recognized the loxP sequence, deleting the *Ubap2*^{flox} region (Figure 1A). To generate the knock-out *Ubap2*$^{flox/flox}$; *Pdx1-Cre* line, male *Ubap2*$^{flox/wt}$ mice were bred with female *Pdx1-Cre* to generate *Ubap2* heterozygous line (*Ubap2*$^{flox/wt}$; *Pdx1-Cre*). Heterozygous *Ubap2*$^{flox/wt}$; *Pdx1-Cre* are then back crossed with *Ubap2*$^{flox/wt}$ mice to generate homozygous *Ubap2*$^{flox/flox}$; *Pdx1-Cre* (**U2KO**). To confirm our knock-out mice, PCR analysis of the *Ubap2* exon five region showed a 250bp fragment for the wild-type allele while the *Ubap2*^{flox} allele was 415bp in size (Figure 1B). For *Pdx1-Cre*, the genotyping PCR amplification resulted in Cre amplification at approximately 650bp. While the internal positive control

amplified the wild-type *Pdx1* gene at 415 bp (Figure 1B). Together, these PCR analyses indicate successful deletion of exon 5 within *Ubap2*. Hematoxylin and eosin (H&E) staining of pancreatic sections of *Ubap2*$^{flox/flox}$ and U2KO male and female mice revealed no observable differences in the tissue architecture (Figure 1C). We probed for *Ubap2* gene knockout through DNA isolation of U2KO pancreatic whole tissue lysates and confirmed the deletion of exon 5 in the genome in our knockout animals (Figure 1D). The U2KO mice appeared grossly normal. U2KO pups did not show any significant phenotypic differences compared to their homozygous wild type (*Ubap2*$^{flox/flox}$) and heterozygous littermates (*Ubap2*$^{flox/wt}$*; Pdx1-Cre*) at day postpartum (P1). Weight gain was not significantly affected when stratifying by either sex (n = 20/genotype) or age (n = 20/genotype) (Figure S1). In summary, we successfully generated a pancreas-specific knockout of *Ubap2* mouse line with no observable differences in the pancreatic tissue histology between the U2KO mice and their wild-type littermates.

Glucose homeostasis in *Ubap2* knock-out mice

Since we did not observe histological differences in the pancreatic tissue of U2KO mice through H&E staining, next we wanted to investigate impact of UBAP2 deletion in normal pancreatic function. Many clinical pancreatic disorders, such as chronic pancreatitis are typically diagnosed after clinical observations of aberrant glycemic control [28]. To determine any role of UBAP2 in glucose homeostasis, oral glucose tolerance tests (OGTT), intraperitoneal glucose tolerance tests (IP-GTT) and insulin tolerance tests (ITT) experiments were performed in males and female mice at three and six months of age [29–31]. Basal glucose levels were not significantly different from each other ($p > 0.05$) (Figure 2A). During the OGTT, blood glucose levels reportedly demonstrated a maximum peak at 30 minutes post gavage, and then normalizing to basal levels by 120 minutes post gavage [32]. In all animals, the glucose spike observed at 30 minutes post gavage was similar between 3- and 6-month-old U2KO and WT female mice. However, in 6-month male mice, the blood glucose levels remained slightly elevated ($p = 0.0379$), suggestive of mild glucose intolerance. Similarly, insulin tolerance tests (ITT) revealed a significant increase across time ($p = 0.0484$). In all animals, we observed an expected blood glucose peak at approximately 30 minutes post insulin injection with no significant differences in our female mice (3- and 6-month) and our 3-month male mice (Figure 2C-D). IP glucose tolerance tests (IP-GTT) showed an increase in the plasma glucose levels in U2KO animals (Figure 3A-B). We observed the largest change in the 3-month female mice group ($p = 0.0048$) (Figure 3A *top row*). Given the mild glucose intolerance, particularly in the 6-month-old male mice, we evaluated serum levels of insulin during the OGTT. Interestingly, we found no significant differences in the insulin levels (Figure 3C-D). Combined, these results demonstrate that the glucose homeostasis in U2KO animals are mostly comparable to control animals (*Ubap2*$^{flox/flox}$). However, a decreased glucose clearance without a reduction in insulin levels through both OGTT and ITT tests was observed for 6-month old male U2KO animals when compared to control animals, which is indicative of a mild glucose intolerance.

Exocrine and endocrine marker expression in *Ubap2* knock-out mice

Changes in endocrine and exocrine markers and/or pancreas architecture are indicative of numerous pancreatic disorders (*e.g.* Type-I Diabetes and Pancreatic Exocrine Insufficiency) [33–35]. Therefore, with the knowledge of 6-month animals' mild glucose intolerance, we stained pancreatic tissue sections for endocrine and exocrine functional markers to evaluate the effect of Ubap2 deletion on pancreatic function/architecture. In the islet region of the pancreas, central core insulin producing cells (β-cells) are surrounded by glucagon-positive cells [36]. Islet cells of 6-month-old animals were stained with antibodies directed against insulin and glucagon (Figure 4). We observed no architectural differences within endocrine compartments, indicating a lack of relevance of Ubap2 function on ordered arrangement of the islet cells. Additionally, insulin and glucagon producing cells were observed in the adult pancreas with no changes in either molecule's expression level or cellular localization when comparing the U2KO animals to control animals (*Ubap2*$^{flox/flox}$) (Figure 4). To examine the effect of Ubap2 deletion on exocrine function, expression of the exocrine/acinar cell markers amylase and Carboxypeptidase A1 (Cpa1) were measured in pancreatic tissue sections from mice of both genotypes. Amylase and Cpa1 markers were indistinguishable between U2KO mice and our control mice (Figure 4), which is similar to previous reports on how critical acinar markers potentially do not have an effect on the three pancreatic compartments (acinus, islets, ducts) [37]. While Ubap2 deletion could have an effect on acinar cell function, we did not see any evidence of morphological changes in the interactions of the three pancreatic compartments. Additionally, no significant changes were observed when looking at exocrine and endocrine marker RNA levels (Figure S1B). Taken together, these results indicate that the deletion of Ubap2 in the pancreas had no effect on pancreatic endocrine/exocrine morphology and marker expression.

Extracellular matrix and mucin staining in *Ubap2* knock-out mice

The expression of mucins is correlated with different pancreatic pathophysiology and deregulated mucin production is a hallmark of inflammatory and neoplastic disorders of the pancreas [38]. Next, we investigated any changes in the extracellular matrix and mucin staining to indicate any role in pancreatic pathophysiology. Pancreatic stellate cells (PSCs) under physiological conditions assist the exocrine cell structure by maintaining the normal basement membrane [39]. The expression of α-smooth muscle actin (α-SMA) marks the activation of PSCs [39,40]. Activated cells increase production of the extra cellular matrix (ECM) proteins such as fibronectin and collagens leading to fibrosis [41]. Collagen content in the pancreas was assessed by picrosirius red and Mason's trichrome stain. Sirius red stained collagen around ducts and within the lobular space of the pancreas in both control and U2KO animals (Figure 5). The staining pattern of Sirius Red and Mason's trichrome stain were not different in U2KO animals compared to controls (*Ubap2*$^{flox/flox}$), indicating that deletion of Ubap2 has no effect in the extracellular matrix depositions, as well as lack of effects on fibrotic injury or the activation of PSCs. Mucins in the pancreas contribute to biological processes such as the protection, lubrication, and moisturization of epithelial tissues[42]. However, we observed no change in the acidic mucin or neutral mucin (Alcian blue or PAS stains) in U2KO mice compared to controls in mice of both sexes (Figure 5). These results indicate that Ubap2 deletion has no effect in the pancreas mucin expression. Together, these results demonstrate that Ubap2 deletion in the pancreas does not affect

the maintenance processes of the pancreas; the pancreas was not affected through aberrant collagen secretion, mucin changes, or stellate cell activation.

Cerulein-Induced Pancreatitis in *Ubap2* knock-out mice

Pancreatitis is typically a result of a pancreatic injury (either mechanical or chemical) leading to inflammation and pancreatic enzyme secretion. Cerulein-induced pancreatitis is a well-characterized experimental model that can be tailored to mimic either acute or chronic pancreatitis. Cerulein is an ortholog of cholecystokinin, which given in supramaximal doses, results in inflammatory cytokine induction (IL-1β) and secretion of exocrine pancreatic enzymes, including amylase and lipase, that result in pancreatic injury [43,44]. To assess the relevance of Ubap2 in the pancreatitis response, we induced acute experimental pancreatitis (AP) in mice and observed for changes in tissue damage, enzymatic secretion, and cytokine levels (Figures 6 and S2A). H&E stains of pancreatic sections indicated damage to the pancreatic acini of control animals (*Ubap2*$^{flox/flox}$) as expected. However, the extent of damage to the pancreatic acini was less prominent in U2KO animals (Figure 6A). To further support the extent of tissue damage and to evaluate the innate immune response to AP, we measured neutrophil infiltration into the pancreatic tissue through the expression of myeloperoxidase (Figure 6B-C). Upon AP treatment, neutrophil infiltration into the pancreas of control animals increased approximately 10-fold (Figure 6B, *left*) compared to vehicle controls. However, neutrophil infiltration in cerulein-treated U2KO animals were reduced by 50% compared to cerulein-treated control animals (Figure 6B, *right*). Furthermore, U2KO animals had a significantly inhibited neutrophil infiltration occurrence in the pancreatic tissue compared to control animals ($p = 0.0223$) (Figure 6C), indicating a protection against cerulein-induced pancreatic injury, from an innate immune cell response. When analyzed for changes in acidic mucin or neutral mucin (Alcian blue or PAS stains), cerulein-induced pancreatitis mice were comparable to control mice (Figure S3), indicated by a lack of significant blue or purple color deposition in the tissues. These results suggest that there is no noticeable perturbation in the regulation of ECM component by the presence or deletion of Ubap2.

Aberrant release of amylase and lipase into the circulation are clinical and experimental indications of pancreatitis, and they are phenotypes that are mimicked in AP [45]. In control (*Ubap2*$^{flox/flox}$) mice, we observed the expected phenotypical increase in serum amylase and lipase levels by cerulein treatment compared to a vehicle control, of 2.1-fold ($p = 0.0051$) and 3.2-fold ($p = 0.0366$), respectively, (Figure 6D-E). In U2KO mice, although the basal serum amylase levels were higher in the vehicle control group (AMYL = 6281 U/L) but remained unaffected by cerulein injection (AMYL = 4988 U/L) to a significant degree ($p = 0.21$) (Figure 6D). However, when compared with vehicle-treated control, serum lipase levels in cerulein-treated control animals increased significantly to near clinical levels of pancreatitis. However, cerulein-treatment did not increase the serum lipase levels in U2KO animals when compared with vehicle-treated U2KO animals and the lipase levels were comparable to the vehicle-treated control animals, indicating protection from cerulein-induced pancreatitis in U2KO animals (Figure 6E). Overall, these results indicate that Ubap2 deletion in the pancreas results in a decrease in the pro-inflammatory pancreatitis response

including a lack of change in secreted amylase and lipase enzymes, both of which are clinical and experimental markers of pancreatitis in mice and humans.

Impact on NF-kB activation and inflammatory signaling during Cerulein-Induced pancreatitis

Next, we investigated mechanisms through which Ubap2 deletion reduced cerulein-induced pancreatitis phenotype. Since AP-treated U2KO animals had less neutrophil infiltration into the pancreas and an altered secretion profile, we wanted to see if there were any changes in the cytokine expression profile of the U2KO animals during AP (Figure S2A).

It has been reported that cerulein induce pancreatitis activates NF-kB signaling pathway and activation of NFκB is an early event during pancreatitis [46]. To decipher mechanisms of a role of UBAP2 in cerulein induced pancreatitis, we quantified 40 mouse proteins, including cytokines, chemokines, and growth factors, from the serum of mice treated with either PBS or cerulein and with or without deletion of UBAP2, using Proteome Profiler Mouse Cytokine Array kit. When compared to vehicle controls, the chemoattractant cytokines Cxcl1 and Cxcl13 were increased in *Ubap2*$^{flox/flox}$ animals (2.66- and 3.5-fold respectively), as expected, but these increases were not seen in the U2KO animals (Figure S2A) [47]. The levels of inflammatory cytokine Il1-β increased by 2.24-fold in wild-type cerulein-treated animals, as reported previously, however, Il1-β levels decreased significantly in cerulein-treated U2KO animals (~ 4 fold change) (Figure S2A) [48]. NF-κB has been previously reported to be activated early in acinar cells during AP and results in increased expression of multiple proinflammatory genes, including Il1-β [49]. Our results demonstrated changes in the levels of Il-1β, TNFα, IFN-γ, and Il-10 among others. These specific molecules are known to be direct targets of NF-κB signals [50], [51], [52 & 53]. As a result, next we evaluated NF-κB activation in U2KO mice under AP conditions (Figure 7 and S2B). It is established in the literature that the activation of the NF-kB pathway is linked to the translocation of p65-NF-κB into the nucleus. Once translocated into the nucleus, the p65 subunit of NF-κB initiates transcription[6]. We therefore, analyzed activation of NF-kB pathway by measuring nuclear localization of p65-NF-κB using immunofluorescence. In control animals (*Ubap2*$^{flox/flox}$), immunofluorescence staining for the p65 subunit of NF-κB indicated an approximately 5-fold increase in p65- NF-κB nuclear localization upon AP treatment ($p = 0.0081$), indicating NF-κB activation (Figure S2B, Figure 7A, *left*). In U2KO animals, the same treatment did not induce p65- NF-κB nuclear localization significantly over the vehicle control ($p = 0.3785$) (Figure S2B, Figure 7A, *right*). Nuclear p65-NF-κB levels were significantly lower in U2KO animals compared to control animals receiving AP (Figure 7A-B) ($p = 0.0062$). To further support the mechanisms of decreased Il1-β levels in cerulein-treated U2KO animals, we utilized AR42J acinar cell line to investigate binding of NF-κB to various genomic locations, indicating activity. Chromatin immunoprecipitation (CHIP) assays in the AR42J cell line revealed an increased binding of NF-κB to the Il-1β promoter region as well as the IκBα promoter region, indicating increased Il-1β expression and NF-κB autoregulation [54,55]. However, transient silencing of Ubap2 by siRNA In AR42J cells abolished binding of NF-κB to Il-1β and IκBα promoters (Figure 7C and Figure S2C). These results indicate that UBAP2 maintains a pro-inflammatory niche in cerulein-induced pancreatitis model via activation of NF-κB.

Discussion and Future Directions

In 2020, we described how UBAP2 regulates the activation of KRAS and macropinocytosis in pancreatic cancer[16]. Silencing UBAP2 decreases the levels of activated KRAS, and inhibits macropinocytosis, and tumor growth in vivo. Using a UBAP2-deletion construct, we demonstrated that the UBA-domain of UBAP2 is critical for the regulation of macropinocytosis and maintaining the levels of activated KRAS. UBAP2 was expressed in PDAC and it is mostly localized in the acinar/islet cells of the benign or normal tissues adjacent to the tumor. In summary we concluded that UBAP2 regulates RAS downstream signaling and helps maintain RAS in the GTP-bound form. However, a role for UBAP2 in the healthy pancreas has not been studied, warranting a further study on this molecule in the healthy pancreas. In this report, we generated and characterized a novel mouse model expressing a Ubap2-floxed gene under the control of a pancreas-specific Cre recombinase.

Glucose tolerance tests revealed evidence of increased fasting glucose and reduced glucose clearance in the 6-month, male U2KO animals, indicating an insulin resistance and interference β-cell insulin secretion phenotype, however there was no change in fasting insulin. Impaired glucose clearance was also found on the ITT (Figure 2D, $p = 0.048$) which confirms insulin resistance at 6 months. Taken together, these two tests indicate an impaired glucose tolerance phenotype only in the U2KO 6-month male group. When examining the islet cell histological stains (Figure 4, *bottom*), the insulin levels (Figure 3 C-D), and the expression of pancreatitis gene (Figure S1B), we observed no significant changes in the islet cell mass or insulin secretion during the OGTT. Our data within our male animals is consistent with a recent whole-body, endonuclease-mediated UBAP2 knockout from the Jackson Labs data repository [75], where elevated levels of circulating blood glucose in 3 males were reported[56,57]. In female U2KO mice, there was no difference in fasting glucose or insulin. However, the 3-month U2KO females had significantly elevated glucose determined by the IP-GTT ($p = 0.0048$) with a strong trend for the same increase observed in the 6-month U2KO female animals ($p = 0.0681$) (Figure 3A). This trend was not observed during the oral glucose tolerance test (OGTT, Figure 2A). The reasons for this difference are not known, however differences between routes of glucose administration can affect the glucose metabolism and hence tolerance levels in rodents [58–60], as glucose tolerance following oral glucose loading is influenced by intestinal derived factors that can alter insulin secretion/efficacy; this phenomenon would be absent from intraperitoneal glucose injection [59,61].

When evaluating various endocrine and exocrine components to pancreatic function, we observed that the U2KO animals retained their islet architectural phenotype when compared to the wild-type control animals, seen through insulin and glucagon expression and localization. Pancreatic tissue endocrine and exocrine markers, both show a similar lack of change in our U2KO mice using the markers *Cpa1*, *Amylase*, *Insulin*, *Glucagon*, and *Ck-19* (Figures 4 and 5). Likewise, pancreatic stellate cell activation (α-SMA and ECM stains) revealed that U2KO mice had no significant differences when compared to control animals (Figure 5). This indicates that UBAP2 is not affecting extracellular matrix deposition, and therefore, has likely no effect on the activation of the pancreatic stellate cells.

In our AP model, we observed tissue damage is less pronounced in U2KO animals than controls (Figure 6A) with a corresponding decrease in neutrophil infiltration into the pancreatic tissue (Figure 6B, $p = 0.0223$). The decrease in neutrophil infiltration was reinforced by a decrease of *Cxcl1* in the serum of U2KO animals upon pancreatitis induction when compared to control animals (Figure S2A). Interestingly, we see a decrease in *Cxcl13* which contributes for lymphocyte recruitment due to inflammation, and previously reported to be relevant to PDAC metastasis via ETS variant 4 (ETV4) [62]. The summation of this data indicates a lack of an inflammatory response in U2KO animals, but specifics on the contributions of neutrophil-mediated inflammation versus the acinar cells-mediated inflammation are still debated in the literature[63–65].

Experimental and clinical indicators of an acute pancreatitis response are increases in the levels of serum amylase and lipase[66–68]. We observed the expected increase in both enzymes in our control animals, but serum enzymatic levels of amylase and lipase were unchanged in our U2KO animals. A very interesting observation was the differences in amylase and lipase levels in the U2KO animals. While both enzymes were unchanged with cerulein administration, U2KO animals had higher basal levels of amylase with normal levels of lipase. While experimentally, a vast portion of the literature focuses on the two enzymes elevating together, clinically, there are a few cases of the enzymes indicating different phenotypes like described in our data [69]. This could indicate a niche role for UBAP2 in amylase and lipase secretion pathways, but future work into how this phenotype is relevant to pancreatitis (its progression, severity, and/or recovery) is warranted. Interestingly, the increased serum amylase levels of the U2KO animals could suggest that the circulating factors in these mice, notably amylase [70], or other exocrine dependent factors may interfere with the insulin action in U2KO mice.

We observed an expected increase in circulating Il1-β upon AP in control animals, an observation that was not seen in the U2KO animals (Figure S2A) [48,71,72]. To evaluate how Ubap2 is relevant to Il1-β expression during AP, we measured NF-κB activation (via p65 nuclear localization) during AP (Figure 7A-B). Subsequent ChIP experiments in the *in vitro* AR42J system confirmed NF-κB binding to the genome upon AP at the Il1-β promoter region and the IκB-α promoter region, both which are expected NF-κB binding sites upon activation[55,73] (Figure 7C, S2B). It is reported that the NF-κB activation and translocation to the nucleus is indicative of a AP response [74], but this phenotype is not seen in our U2KO animals that received cerulein (Figure 7A-B). Taken together, this data indicates an effect of UBAP2 on the NF-κB signaling axis. The literature has established the complexity of the NF-κB signaling axis during pancreatitis and the need to carefully examine results from both *in vitro and in vivo* systems to make conclusions is extremely complex and the results here need to be followed up with careful interpretation in both *in vitro* and *in vivo* systems[49,55,75]. For example, NF-κB binding to its negative regulatory gene IκBα has been established previously, as well as its paradoxical nature [73,76]. We established the binding of NF-κB to the IκBα promoter region under a cerulein response, indicating an expected NF-κB activation signal, but that signal was reduced in Ubap2-silenced AR42J cells as expected. Combined with our *in vivo* immunofluorescence data showing a lack of NF-κB translocation to the nuclei in the pancreatic tissue, this data can be interpreted to indicate a positive role of Ubap2 signaling on the NF-κB pathway. Future studies focusing on the

potential for PKC(D) signaling during cerulein induced pancreatitis and direct interaction studies with NF-κB given the importance of ubiquitination in NF-κB signaling will provide additional molecular insight on the role of Ubap2 in cerulein induced pancreatitis [75,77,78].

PDAC develops through the progression of precursor lesions known as pancreatic intraepithelial neoplasia (PanIN). Activating mutations in the KRAS oncogene is the major initiating event in the vast majority of PDAC, as its activation initiate premalignant lesions. Pancreatitis, PanINs are a risk factor for developing pancreatic cancer. Long-standing inflammation increases cell turnover and stellate cell proliferation, this creates a pancreatic tissue microenvironment conducive to carcinogenesis[16]. Our results demonstrate that Ubap2 deletion inhibits cerulein-induced pancreatitis by inhibiting the inflammation. We previously reported that UBAP2 regulates KRAS activation and promotes macropinocytosis. Although a role of macropinocytosis has not been implicated in the initiation of pancreatic cancer, however, we speculate that deletion of UBAP2 will slow down the initiation of KRAS-induced PDAC tumorigenesis. Some of the limitations of this study are the observation of slightly elevated blood glucose levels in 6-month-old U2KO male mice, mechanisms of which are still not clear. Interestingly, in the knockout animal group, we did not observe any noticeable differences in terms of islet cell mass, exocrine and endocrine marker RNAs, or insulin levels. These observations suggest that U2KO male mice may exhibit insulin resistance in the liver or skeletal muscle, which warrants further investigation using a hyperinsulinemic- clamp technique[79]. Another interesting observation is the potential impact of Beta-cell insulin secretion, which is influenced by both direct and indirect inter-organ/inter-cellular communication involving various factors. This may include circulating amylase, which was found to be three times higher in the U2KO mice. The mechanisms of higher amylase levels in U2KO animals are not clear. To gain a deeper understanding of whether Ubap2 knockout interferes with glucose-stimulated insulin secretion, isolated islet testing is warranted. In summary, deletion of UBAP2 in the pancreas indicated minimal changes to glucose intolerance in the pancreas and reduced the inflammatory response during cerulein-induced pancreatitis, through inhibited NF- κB activation in the acinar cells. The results presented together also suggest that UBAP2 may be exploited as a potential therapeutic target to cerulein induced pancreatitis and potentially slowing down pancreatic tumorigenesis in future[80].

Supplementary Material

Refer to Web version on PubMed Central for supplementary material.

Funding:

The authors gratefully acknowledge the funding sources.

National Institutes of Health Grants: CA220237, 2CA136494, CA213278, CA253391, 1R01CA260449–01A1 (PM)

Peggy and Charles Stephenson Cancer Center (PM)

National Institutes of Health Grant P20 GM103639 (Core)

National Cancer Institute Cancer Center Support Grant P30CA225520 (Core)

References

1. Campbell JE & Newgard CB Mechanisms controlling pancreatic islet cell function in insulin secretion. Nature Reviews Molecular Cell Biology 22, 142–158, doi:10.1038/s41580-020-00317-7 (2021). [PubMed: 33398164]
2. Gittes GK Developmental biology of the pancreas: A comprehensive review. Developmental Biology 326, 4–35, doi:10.1016/j.ydbio.2008.10.024 (2009). [PubMed: 19013144]
3. Husain S. & Thrower E. Molecular and cellular regulation of pancreatic acinar cell function. Curr Opin Gastroenterol 25, 466–471, doi:10.1097/MOG.0b013e32832ebfac (2009). [PubMed: 19571746]
4. Gukovskaya AS et al. Pancreatic acinar cells produce, release, and respond to tumor necrosis factor-alpha. Role in regulating cell death and pancreatitis. J Clin Invest 100, 1853–1862, doi:10.1172/jci119714 (1997). [PubMed: 9312187]
5. Da Silva Xavier G. The Cells of the Islets of Langerhans. Journal of Clinical Medicine 7, 54 (2018). [PubMed: 29534517]
6. Leung PS & Ip SP Pancreatic acinar cell: Its role in acute pancreatitis. The International Journal of Biochemistry & Cell Biology 38, 1024–1030, doi:10.1016/j.biocel.2005.12.001 (2006). [PubMed: 16423553]
7. Mayerle J. et al. Metabolic biomarker signature to differentiate pancreatic ductal adenocarcinoma from chronic pancreatitis. Gut 67, 128–137, doi:10.1136/gutjnl-2016-312432 (2018). [PubMed: 28108468]
8. Carrière C, Young AL, Gunn JR, Longnecker DS & Korc M. Acute pancreatitis accelerates initiation and progression to pancreatic cancer in mice expressing oncogenic Kras in the nestin cell lineage. PloS one 6, e27725e27725, doi:10.1371/journal.pone.0027725 (2011).
9. He R. et al. SULF2 enhances GDF15-SMAD axis to facilitate the initiation and progression of pancreatic cancer. Cancer Letters 538, 215693, doi:10.1016/j.canlet.2022.215693 (2022).
10. Wolfgang CL et al. Recent progress in pancreatic cancer. CA Cancer J Clin 63, 318–348, doi:10.3322/caac.21190 (2013). [PubMed: 23856911]
11. Aier I., Semwal R., Sharma A. & Varadwaj PK. A systematic assessment of statistics, risk factors, and underlying features involved in pancreatic cancer. Cancer Epidemiology 58, 104–110, doi:10.1016/j.canep.2018.12.001 (2019). [PubMed: 30537645]
12. Ma Y, Nikfarjam M. & He H. The trilogy of P21 activated kinase, autophagy and immune evasion in pancreatic ductal adenocarcinoma. Cancer Letters 548, 215868, doi:10.1016/j.canlet.2022.215868 (2022).
13. Li T-J et al. SIGLEC15 amplifies immunosuppressive properties of tumor-associated macrophages in pancreatic cancer. Cancer Letters 530, 142–155, doi:10.1016/j.canlet.2022.01.026 (2022). [PubMed: 35077803]
14. Pan S, Brentnall TA & Chen R. Proteome alterations in pancreatic ductal adenocarcinoma. Cancer Letters 469, 429–436, doi:10.1016/j.canlet.2019.11.020 (2020). [PubMed: 31734355]
15. Buscail L, Bournet B. & Cordelier P. Role of oncogenic KRAS in the diagnosis, prognosis and treatment of pancreatic cancer. Nature Reviews Gastroenterology & Hepatology 17, 153–168, doi:10.1038/s41575-019-0245-4 (2020). [PubMed: 32005945]
16. Xiong X. et al. Ubiquitin-binding associated protein 2 regulates KRAS activation and macropinocytosis in pancreatic cancer. The FASEB Journal 34, 12024–12039, doi:10.1096/fj.201902826RR (2020).
17. Longo M. et al. Adverse Effect of High-Fat Diet on Metabolic Programming in Offspring Born to a Murine Model of Maternal Hypertension. American Journal of Hypertension 29, 1366–1373, doi:10.1093/ajh/hpw088 (2016). [PubMed: 27565786]
18. Andrikopoulos S, Blair AR, Deluca N, Fam BC & Proietto J. Evaluating the glucose tolerance test in mice. American Journal of Physiology-Endocrinology and Metabolism 295, E1323-E1332, doi:10.1152/ajpendo.90617.2008 (2008).
19. Carper D, Coué M, Laurens C, Langin D. & Moro C. Reappraisal of the optimal fasting time for insulin tolerance tests in mice. Molecular Metabolism 42, 101058, doi:10.1016/j.molmet.2020.101058 (2020).

20. Kemkem Y. et al. Maternal hypothyroidism in mice influences glucose metabolism in adult offspring. Diabetologia 63, 1822–1835, doi:10.1007/s00125-020-05172-x (2020). [PubMed: 32472193]
21. Au - Nagy C. & Au - Einwallner E. Study of In Vivo Glucose Metabolism in High-fat Diet-fed Mice Using Oral Glucose Tolerance Test (OGTT) and Insulin Tolerance Test (ITT). JoVE, e56672, doi:doi:10.3791/56672 (2018).
22. Song Y. et al. Gut-Proglucagon-Derived Peptides Are Essential for Regulating Glucose Homeostasis in Mice. Cell Metabolism 30, 976–986.e973, doi:10.1016/j.cmet.2019.08.009 (2019).
23. Hyun JJ & Lee HS Experimental models of pancreatitis. Clin Endosc 47, 212–216, doi:10.5946/ce.2014.47.3.212 (2014). [PubMed: 24944983]
24. Lerch MM & Gorelick FS Models of Acute and Chronic Pancreatitis. Gastroenterology 144, 1180–1193, doi:10.1053/j.gastro.2012.12.043 (2013). [PubMed: 23622127]
25. Sah RP, Dudeja V, Dawra RK & Saluja AK Cerulein-Induced Chronic Pancreatitis Does Not Require Intra-Acinar Activation of Trypsinogen in Mice. Gastroenterology 144, 1076–1085.e1072, doi:10.1053/j.gastro.2013.01.041 (2013).
26. Norkina O, Graf R, Appenzeller P. & De Lisle RC Caerulein-induced acute pancreatitis in mice that constitutively overexpress Reg/PAPgenes. BMC Gastroenterology 6, 16, doi:10.1186/1471-230X-6-16 (2006). [PubMed: 16700916]
27. Magnuson Mark A. & Osipovich Anna B. Pancreas-Specific Cre Driver Lines and Considerations for Their Prudent Use. Cell Metabolism 18, 9–20, doi:10.1016/j.cmet.2013.06.011 (2013). [PubMed: 23823474]
28. Sharma A, Smyrk TC, Levy MJ, Topazian MA & Chari ST Fasting Blood Glucose Levels Provide Estimate of Duration and Progression of Pancreatic Cancer Before Diagnosis. Gastroenterology 155, 490–500.e492, doi:10.1053/j.gastro.2018.04.025 (2018).
29. Ayala JE et al. Standard operating procedures for describing and performing metabolic tests of glucose homeostasis in mice. Dis Model Mech 3, 525–534, doi:10.1242/dmm.006239 (2010). [PubMed: 20713647]
30. Brach S. et al. . Genetic Nicotinamide N-Methyltransferase (Nnmt) Deficiency in Male Mice Improves Insulin Sensitivity in Diet-Induced Obesity but Does Not Affect Glucose Tolerance. Diabetes 68, 527–542, doi:10.2337/db18-0780 (2019). [PubMed: 30552109]
31. Li S. et al. Naringenin improves insulin sensitivity in gestational diabetes mellitus mice through AMPK. Nutr Diabetes 9, 28, doi:10.1038/s41387-019-0095-8 (2019). [PubMed: 31591391]
32. Gelling RW et al. Lower blood glucose, hyperglucagonemia, and pancreatic alpha cell hyperplasia in glucagon receptor knockout mice. Proc Natl Acad Sci U S A 100, 1438–1443, doi:10.1073/pnas.0237106100 (2003). [PubMed: 12552113]
33. Adams MT, Gilbert JM, Hinojosa Paiz J, Bowman FM & Blum B. Endocrine cell type sorting and mature architecture in the islets of Langerhans require expression of Roundabout receptors in β cells. Scientific Reports 8, 10876, doi:10.1038/s41598-018-29118-x (2018).
34. Campbell-Thompson M, Rodriguez-Calvo T. & Battaglia M. Abnormalities of the Exocrine Pancreas in Type 1 Diabetes. Current Diabetes Reports 15, 79, doi:10.1007/s11892-015-0653-y (2015). [PubMed: 26318606]
35. Vujasinovic M, Valente R, Del Chiaro M, Permert J. & Löhr J-M Pancreatic Exocrine Insufficiency in Pancreatic Cancer. Nutrients 9, 183 (2017). [PubMed: 28241470]
36. Zhu L. et al. Intraislet glucagon signaling is critical for maintaining glucose homeostasis. Jci Insight 4, doi: ARTN e127994 10.1172/jci.insight.127994 (2019).
37. Fleming Martinez AK & Storz P. Mimicking and Manipulating Pancreatic Acinar-to-Ductal Metaplasia in 3dimensional Cell Culture. J Vis Exp, doi:10.3791/59096 (2019).
38. Kaur S, Kumar S, Momi N, Sasson AR & Batra SK Mucins in pancreatic cancer and its microenvironment. Nature Reviews Gastroenterology & Hepatology 10, 607–620, doi:10.1038/nrgastro.2013.120 (2013). [PubMed: 23856888]
39. Pang TCY, Wilson JS & Apte MV Pancreatic stellate cells: what's new? Curr Opin Gastroenterol 33, 366–373, doi:10.1097/MOG.0000000000000378 (2017). [PubMed: 28590306]

40. Li Y-X et al. ACLP promotes activation of cancer-associated fibroblasts and tumor metastasis via ACLP-PPARγ-ACLP feedback loop in pancreatic cancer. Cancer Letters 544, 215802, doi:10.1016/j.canlet.2022.215802 (2022).
41. Krah NM et al. The acinar differentiation determinant PTF1A inhibits initiation of pancreatic ductal adenocarcinoma. Elife 4, doi:10.7554/eLife.07125 (2015).
42. Suh H, Pillai K. & Morris DL Mucins in pancreatic cancer: biological role, implications in carcinogenesis and applications in diagnosis and therapy. Am J Cancer Res 7, 1372–1383 (2017). [PubMed: 28670497]
43. Zhang H. et al. Astaxanthin ameliorates cerulein-induced acute pancreatitis in mice. International Immunopharmacology 56, 18–28, doi:10.1016/j.intimp.2018.01.011 (2018). [PubMed: 29328945]
44. Jeong YK & Kim H. A Mini-Review on the Effect of Docosahexaenoic Acid (DHA) on Cerulein-Induced and Hypertriglyceridemic Acute Pancreatitis. International Journal of Molecular Sciences 18, doi:10.3390/ijms18112239 (2017).
45. Jensen RT, Wank SA, Rowley WH, Sato S. & Gardner JD Interaction of CCK with pancreatic acinar cells. Trends in Pharmacological Sciences 10, 418–423, doi:10.1016/0165-6147(89)90192-2 (1989). [PubMed: 2694538]
46. Mayerle J. et al. Genetics, Cell Biology, and Pathophysiology of Pancreatitis. Gastroenterology 156, 1951-+, doi:10.1053/j.gastro.2018.11.081 (2019).
47. Lee KE, Spata M, Maduka R, Vonderheide RH & Simon MC Hif1α Deletion Limits Tissue Regeneration via Aberrant B Cell Accumulation in Experimental Pancreatitis. Cell Rep 23, 3457–3464, doi:10.1016/j.celrep.2018.05.071 (2018). [PubMed: 29924990]
48. Marrache F. et al. Overexpression of Interleukin-1β in the Murine Pancreas Results in Chronic Pancreatitis. Gastroenterology 135, 1277–1287, doi:10.1053/j.gastro.2008.06.078 (2008). [PubMed: 18789941]
49. Huang H. et al. Activation of nuclear factor-κB in acinar cells increases the severity of pancreatitis in mice. Gastroenterology 144, 202–210, doi:10.1053/j.gastro.2012.09.059 (2013). [PubMed: 23041324]
50. Scholz CC et al. Regulation of IL-1beta-induced NF-kappaB by hydroxylases links key hypoxic and inflammatory signaling pathways. Proc Natl Acad Sci U S A 110, 18490–18495, doi:10.1073/pnas.1309718110 (2013).
51. Hayden MS & Ghosh S. Regulation of NF-kappa B by TNF family cytokines. Semin Immunol 26, 253–266, doi:10.1016/j.smim.2014.05.004 (2014). [PubMed: 24958609]
52. Pfeffer LM The Role of Nuclear Factor kappa B in the Interferon Response. J Interf Cytok Res 31, 553–559, doi:10.1089/jir.2011.0028 (2011).
53. Driessler F, Venstrom K, Sabat R, Asadullah K. & Schottelius AJ Molecular mechanisms of interleukin-10-mediated inhibition of NF-kappaB activity: a role for p50. Clin Exp Immunol 135, 64–73, doi:10.1111/j.1365-2249.2004.02342.x (2004). [PubMed: 14678266]
54. Charrier A, Chen R, Kemper S. & Brigstock DR Regulation of pancreatic inflammation by connective tissue growth factor (CTGF/CCN2). Immunology 141, 564–576, doi:10.1111/imm.12215 (2014). [PubMed: 24754049]
55. Ferreiro DU & Komives EA Molecular mechanisms of system control of NF-kappaB signaling by IkappaBalpha. Biochemistry 49, 1560–1567, doi:10.1021/bi901948j (2010). [PubMed: 20055496]
56. Virtue S. & Vidal-Puig A. GTTs and ITTs in mice: simple tests, complex answers. Nature Metabolism 3, 883–886, doi:10.1038/s42255-021-00414-7 (2021).
57. Au - Ayala JE et al. Hyperinsulinemic-euglycemic Clamps in Conscious, Unrestrained Mice. JoVE, e3188, doi:doi:10.3791/3188 (2011).
58. Pilon S., Holloway AC. & Thomson EM. Metabolic, stress, and inflammatory biomarker responses to glucose administration in Fischer-344 rats: intraperitoneal vs. oral delivery. Journal of Pharmacological and Toxicological Methods 90, 1–6, doi:10.1016/j.vascn.2017.10.010 (2018). [PubMed: 29103948]
59. Watada S. et al. Evaluation of Intragastric Vs Intraperitoneal Glucose Tolerance Tests in the Evaluation of Insulin Resistance in a Rodent Model of Burn Injury and Glucagon-Like Polypeptide-1 Treatment. Journal of Burn Care & Research 35, e66–e72, doi:10.1097/BCR.0b013e31828a8ede (2014). [PubMed: 23511296]

60. Small L. et al. Comparative analysis of oral and intraperitoneal glucose tolerance tests in mice. Molecular Metabolism 57, 101440, doi:10.1016/j.molmet.2022.101440 (2022).
61. Vannan DT, Bomhof MR & Reimer RA Comparison of Glucose and Satiety Hormone Response to Oral Glucose vs. Two Mixed-Nutrient Meals in Rats. Frontiers in Nutrition 5, doi:10.3389/fnut.2018.00089 (2018).
62. Gao X. et al. ETV4 promotes pancreatic ductal adenocarcinoma metastasis through activation of the CXCL13/CXCR5 signaling axis. Cancer Letters 524, 42–56, doi:10.1016/j.canlet.2021.09.026 (2022). [PubMed: 34582976]
63. Hirota M. et al. Neutrophil Infiltration and Acinar-ductal Metaplasia Are the Main Pathological Findings in Pembrolizumab-induced Pancreatitis. Intern Med 61, 3675–3682, doi:10.2169/internalmedicine.9565-22 (2022). [PubMed: 35527030]
64. Merza M. et al. Neutrophil Extracellular Traps Induce Trypsin Activation, Inflammation, and Tissue Damage in Mice With Severe Acute Pancreatitis. Gastroenterology 149, 1920–1931.e1928, doi:10.1053/j.gastro.2015.08.026 (2015).
65. Zhou X. et al. Damage associated molecular patterns and neutrophil extracellular traps in acute pancreatitis. Frontiers in Cellular and Infection Microbiology 12, doi:10.3389/fcimb.2022.927193 (2022).
66. Benini L. et al. Variations in time of serum pancreatic enzyme levels in chronic pancreatitis and clinical course of the disease. Int J Pancreatol 8, 279–287, doi:10.1007/bf02952721 (1991). [PubMed: 1724259]
67. Logsdon CD, Moessner J, Williams JA & Goldfine ID Glucocorticoids increase amylase mRNA levels, secretory organelles, and secretion in pancreatic acinar AR42J cells. Journal of Cell Biology 100, 1200–1208, doi:10.1083/jcb.100.4.1200 (1985). [PubMed: 2579957]
68. Suzuki S, Miyasaka K, Jimi A. & Funakoshi A. Induction of acute pancreatitis by cerulein in human IL-6 gene transgenic mice. Pancreas 21, 86–92, doi:10.1097/00006676-200007000-00056 (2000). [PubMed: 10881937]
69. Ismail OZ & Bhayana V. Lipase or amylase for the diagnosis of acute pancreatitis? Clinical Biochemistry 50, 1275–1280, doi:10.1016/j.clinbiochem.2017.07.003 (2017). [PubMed: 28720341]
70. Zhuang L. et al. Serum Amylase Levels in Relation to Islet β Cell Function in Patients with Early Type 2 Diabetes. PLOS ONE 11, e0162204, doi:10.1371/journal.pone.0162204 (2016).
71. Das S, Shapiro B, Vucic EA, Vogt S. & Bar-Sagi D. Tumor Cell–Derived IL1β Promotes Desmoplasia and Immune Suppression in Pancreatic Cancer. Cancer Research 80, 1088–1101, doi:10.1158/0008-5472.Can-19-2080 (2020). [PubMed: 31915130]
72. Takahashi R. et al. Interleukin-1β-induced pancreatitis promotes pancreatic ductal adenocarcinoma via B lymphocyte–mediated immune suppression. Gut 70, 330–341, doi:10.1136/gutjnl-2019-319912 (2021). [PubMed: 32393543]
73. Chiao PJ, Miyamoto S. & Verma IM Autoregulation of I kappa B alpha activity. Proceedings of the National Academy of Sciences 91, 28–32, doi:doi:10.1073/pnas.91.1.28 (1994).
74. Altavilla D. et al. Attenuated Cerulein-Induced Pancreatitis in Nuclear Factor–κB–Deficient Mice. Laboratory Investigation 83, 1723–1732, doi:10.1097/01.LAB.0000101734.82054.BE (2003). [PubMed: 14691290]
75. Yuan J. et al. Novel Small Molecule Inhibitors of Protein Kinase D Suppress NF-kappaB Activation and Attenuate the Severity of Rat Cerulein Pancreatitis. Frontiers in Physiology 8, doi:10.3389/fphys.2017.01014 (2017).
76. Peng B. et al. . Defective feedback regulation of NF-κB underlies Sjögren's syndrome in mice with mutated κB enhancers of the IκBα promoter. Proceedings of the National Academy of Sciences 107, 15193–15198, doi:doi:10.1073/pnas.1005533107 (2010).
77. Hayden MS & Ghosh S. Shared Principles in NF-κB Signaling. Cell 132, 344–362, doi:10.1016/j.cell.2008.01.020 (2008). [PubMed: 18267068]
78. Yuan J. & Pandol SJ PKD signaling and pancreatitis. Journal of Gastroenterology 51, 651–659, doi:10.1007/s00535-016-1175-3 (2016). [PubMed: 26879861]

79. Backdahl J. et al. Spatial mapping reveals human adipocyte subpopulations with distinct sensitivities to insulin. Cell Metab 33, 1869–1882 e1866, doi:10.1016/j.cmet.2021.07.018 (2021). [PubMed: 34380013]

80. Yan HH et al. ANGPTL4 accelerates KRASG12D-Induced acinar to ductal metaplasia and pancreatic carcinogenesis. Cancer Letters 519, 185–198, doi:10.1016/j.canlet.2021.07.036 (2021). [PubMed: 34311032]

Highlights

- UBAP2 is reported to promote macropinocytosis and pancreatic adenocarcinoma (PDAC) growth, however, its role in normal pancreatic function remains unknown.
- We are presenting the initial characterization of pancreatic specific knockout of UBAP2 (U2KO) transgenic mice, marking the first instance of reporting on UBAP2 knockout (U2KO) in the pancreas.
- In the knockout mice pancreatic architecture remained intact, but they demonstrated slight glucose intolerance compared to controls.
- Deletion of UBAP2 protects pancreas from cerulein induced pancreatitis. Mechanistically, cerulein-challenged UBAP2 knockout mice reduced NF-κB activation.

Statement of Significance:

UBAP2 is a new regulator of inflammation and deletion of UBAP2 in pancreas specific manner protects pancreas from cerulein induced pancreatitis.

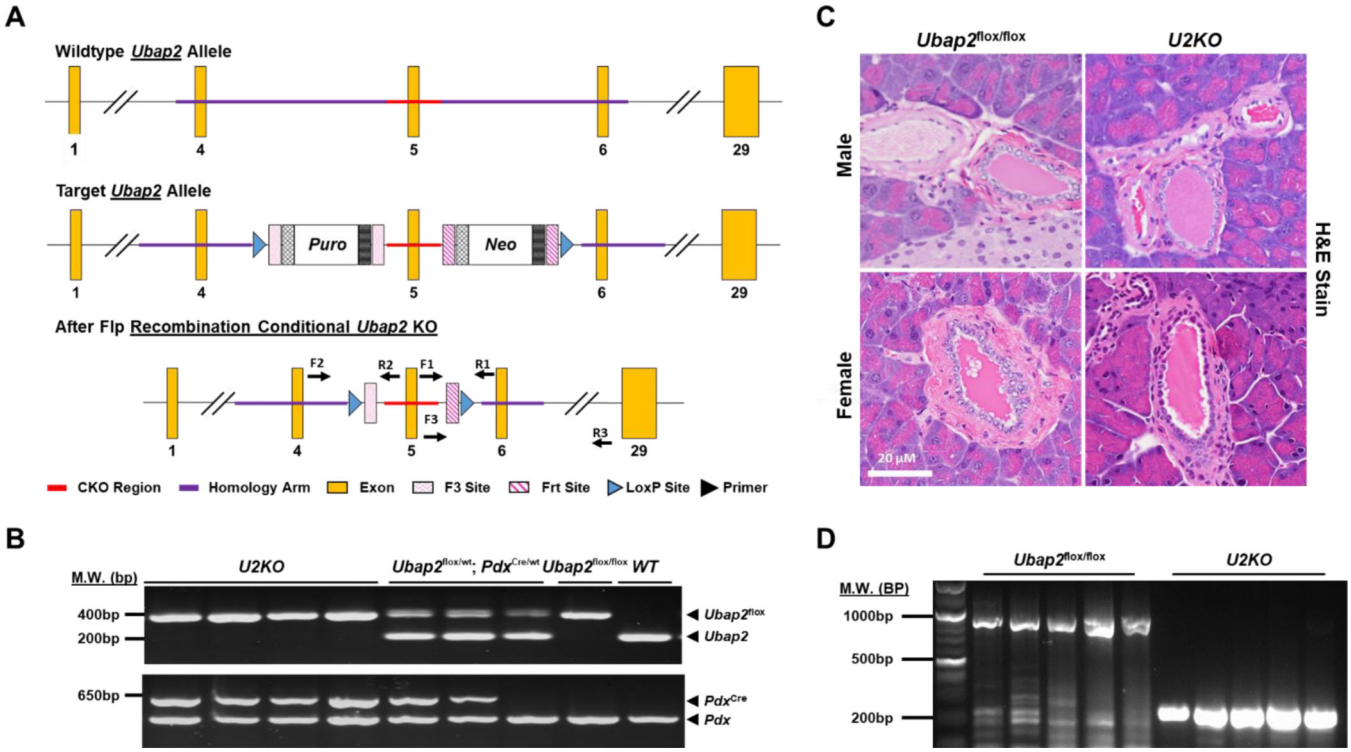

Figure 1. Generation and characterization of *Ubap2* knock-out mice.

(**A**) Schematic representation of the targeting strategy. Mouse line that carries a floxed *Ubap2* (exon 5) coding region flanked by two *loxP*-recognition sites for Cre recombinase. Flp recombinase-activity led to deletion of the selection cassette resulting in a *Ubap2* floxed allele (*Ubap2*^{flox}). (**B**) PCR analysis of the transgenic mice from the DNA isolated from the tail snip. PCR of exon five region showed a 250bp fragment for the wild-type allele while the *Ubap2*^{flox} allele was 415bp in size. For *Pdx-1-Cre*, PCR amplification resulted in 650 bp, while the internal positive control amplified the wild-type *Pdx* gene at 415 bp. (**C**) H&E Staining of pancreatic tissue sections in *Ubap2*$^{flox/flox}$ and U2KO animals. (**D**) DNA analysis of *Ubap2* from whole-cell lysates of the pancreas (N=10).

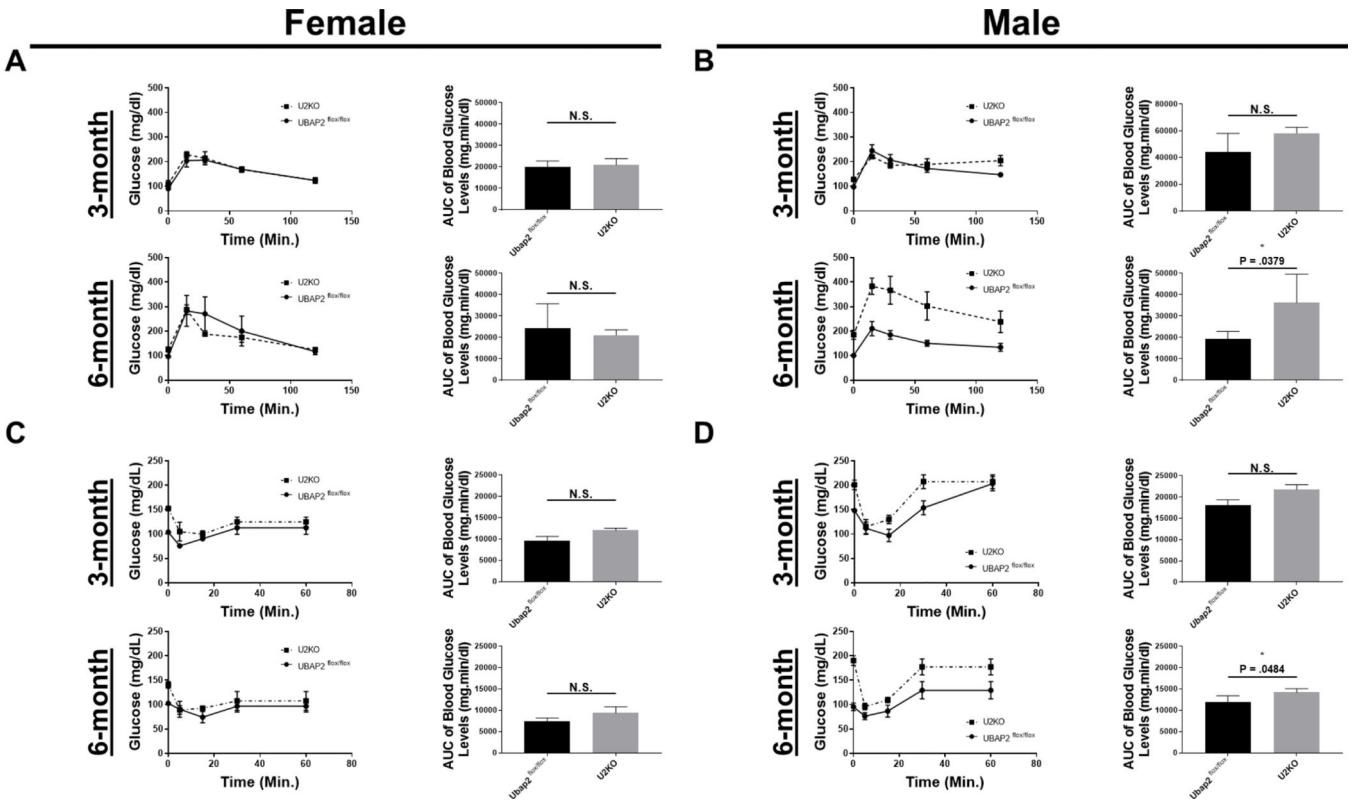

Figure 2. OGTT (A-B) and ITT (C-D) in *Ubap2*$^{flox/flox}$ and *U2KO* animals, stratified by age and sex, with a chow-fed diet.

(A-B) Glucose levels during OGTT experiments. After a 12 hour fast, animals received an I.P. injection of 1g/kg aqueous glucose. The blood glucose levels (mg/dL) were measured at different time points using a glucometer. **(C-D)** Glucose levels during ITT experiments. After a 12 hour fast, animals received an I.P. injection of 0.75 UI/kg. The blood glucose levels (mg/dL) were measured at different time points using a glucometer. (**A-D**) Glucose area under the curve (AUC) were generated through a baseline (Y=0) and ignoring peaks less than 10% of the distance from min-max of Y. The AUC of Blood glucose levels was analyzed via an ordinary One-Way ANOVA with Multiple Comparisons to the Control (*Ubap2*$^{flox/flox}$) of each stratification category. Data are expressed as mean ± standard error of the mean (SEM), n=5–7. All analyses were performed through GraphPad-PRISM (7.04) (* = P < 0.01).

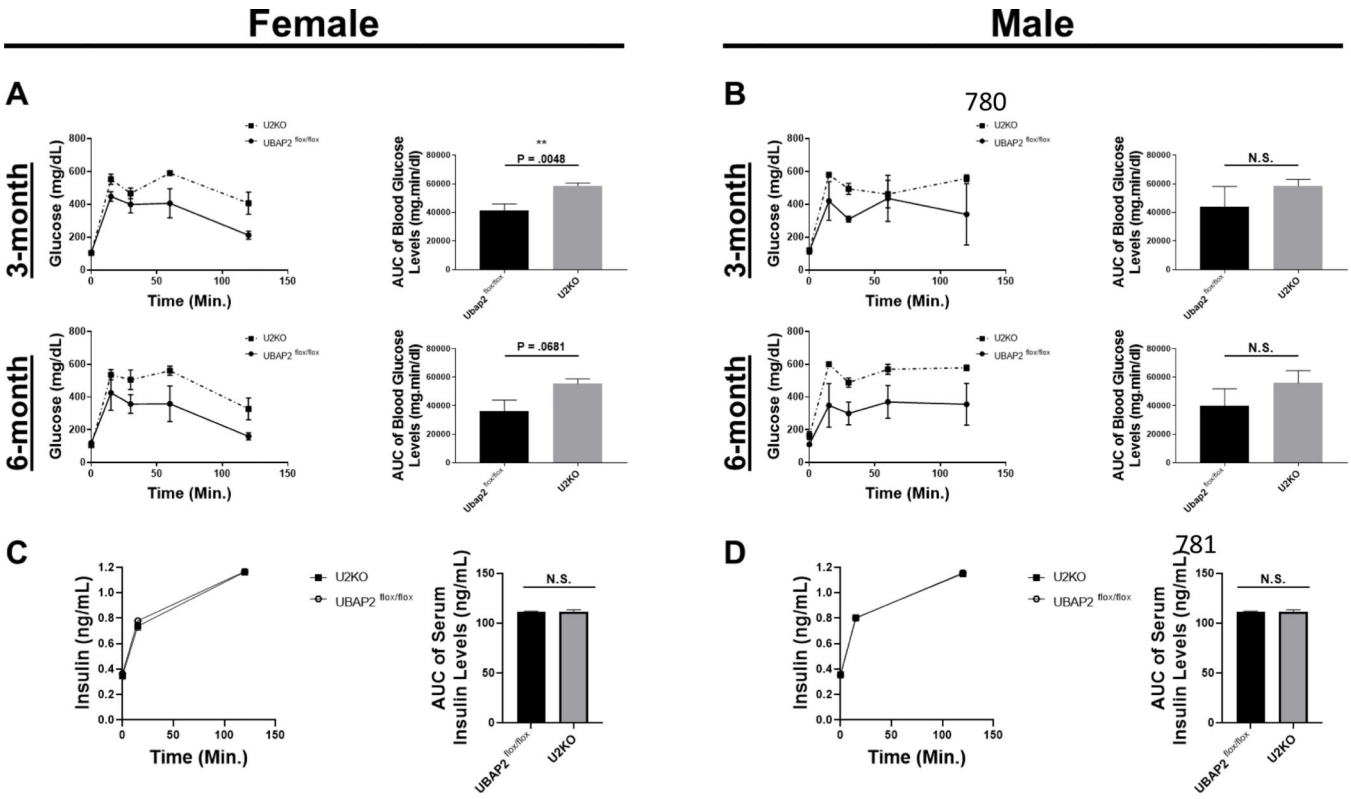

Figure 3. IP-GTT (A-B) and Serum Insulin ELISA levels (C-D) in *Ubap2*$^{flox/flox}$ and *U2KO*, stratified by age and sex, with a chow-fed diet.

(A-B) Glucose levels during IP-GTT experiments. After a 12 hour fast, animals received a dose 1g/kg aqueous glucose delivered into the stomach through a gavage probe. The blood glucose levels (mg/dL) were measured at different time points using a glucometer. Glucose area under the curve (AUC) were generated through a baseline (Y=0) and ignoring peaks less than 10% of the distance from min-max of Y. The AUC of Blood glucose levels was analyzed via an ordinary One-Way ANOVA with Multiple Comparisons to the Control (*Ubap2*$^{flox/flox}$) of each stratification category. Data are expressed as mean ± standard error of the mean (SEM), n=5–7. **(C-D)** Serum Insulin levels through ELISA in 6-month animals stratified by sex. Comparisons were made with the Student'sT-test. Data are expressed as mean ± standard error of the mean (SEM), n=5–7. All analyses were performed through GraphPad-PRISM (7.04) (N.S. = Not significant).

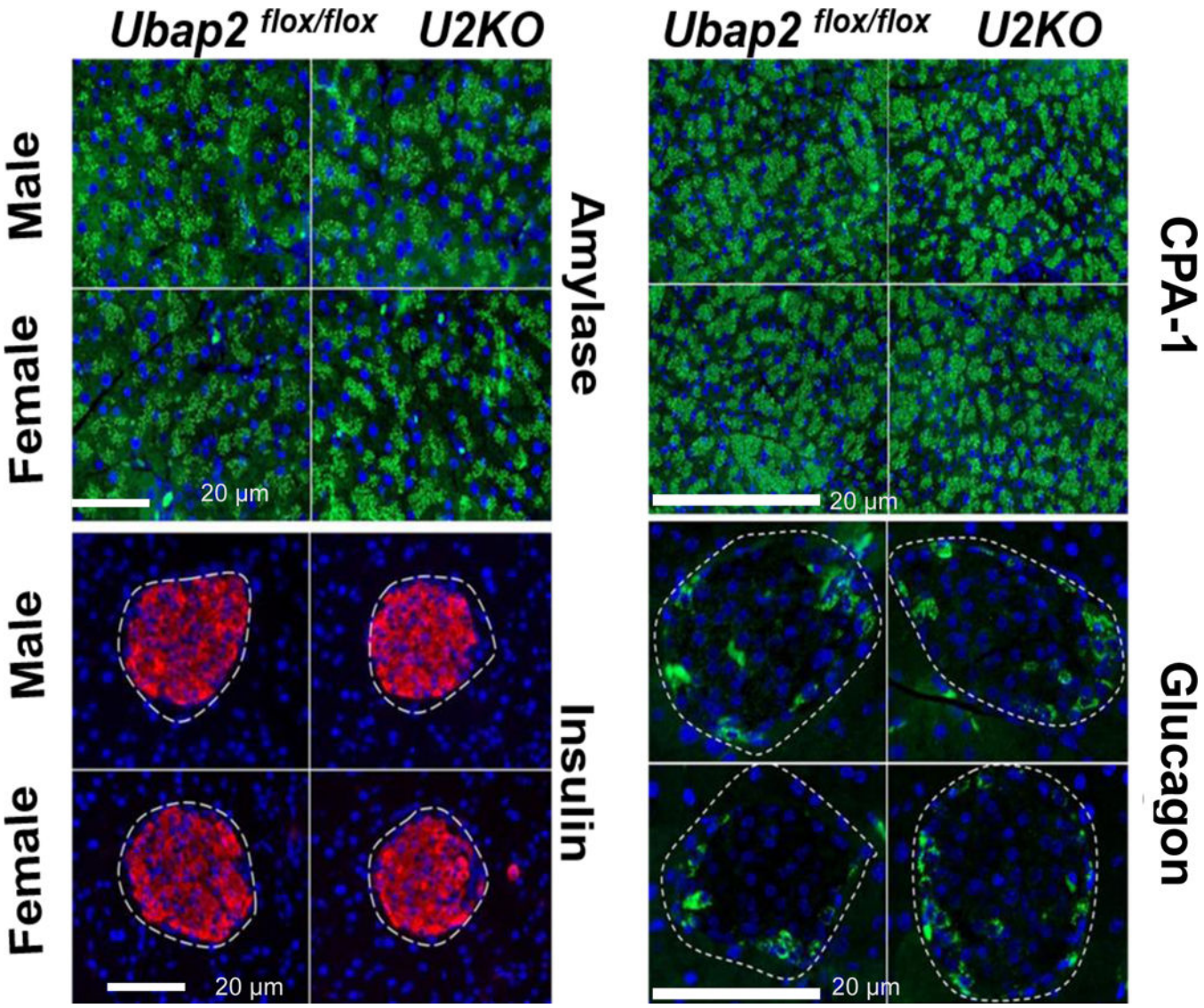

Figure 4. Representative images of pancreatic tissue sections in *Ubap2*$^{flox/flox}$ and *U2KO* animals stained for exocrine [*Top: (L)* Amylase and *(R)* Cpa1] and endocrine [*Bottom: (L)* Insulin and *(R)* Glucagon] genes.

There were no histological differences in the exocrine or endocrine staining between genotypes in mice when stratified by both sex and age. Scale bars: 20μm. Amylase, Cpa1, and glucagon are represented in green. Insulin represented in red. Nuclei were stained with DAPI (blue).

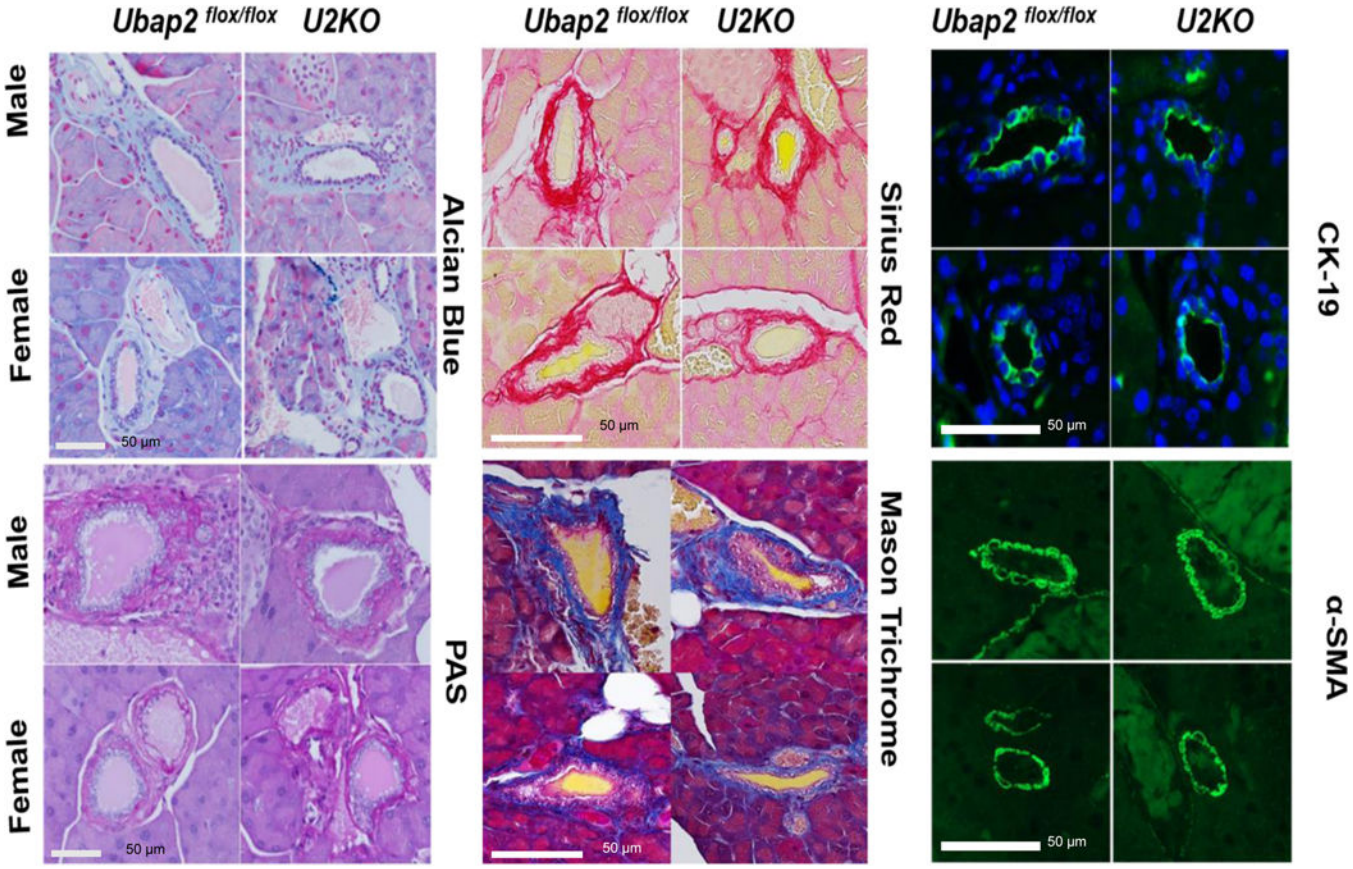

Figure 5. Representative images of pancreatic tissue sections staining for Extracellular matrix and mucin in *Ubap2*$^{flox/flox}$ and *U2KO* animals.

Mucin content were assessed by Alcian Blue stains (*Top row, left column*) and PAS stains (bottom row, left column). Collagen content in the pancreas was assessed by Sirius red (*Top row, middle column*) and Mason's trichrome stain (*Bottom row, middle column*). The expression of α-smooth muscle actin (α-SMA) were depicted in (*Bottom row, Right column*) and expression of CK-19 were shown in the (*Top row, Right column*).

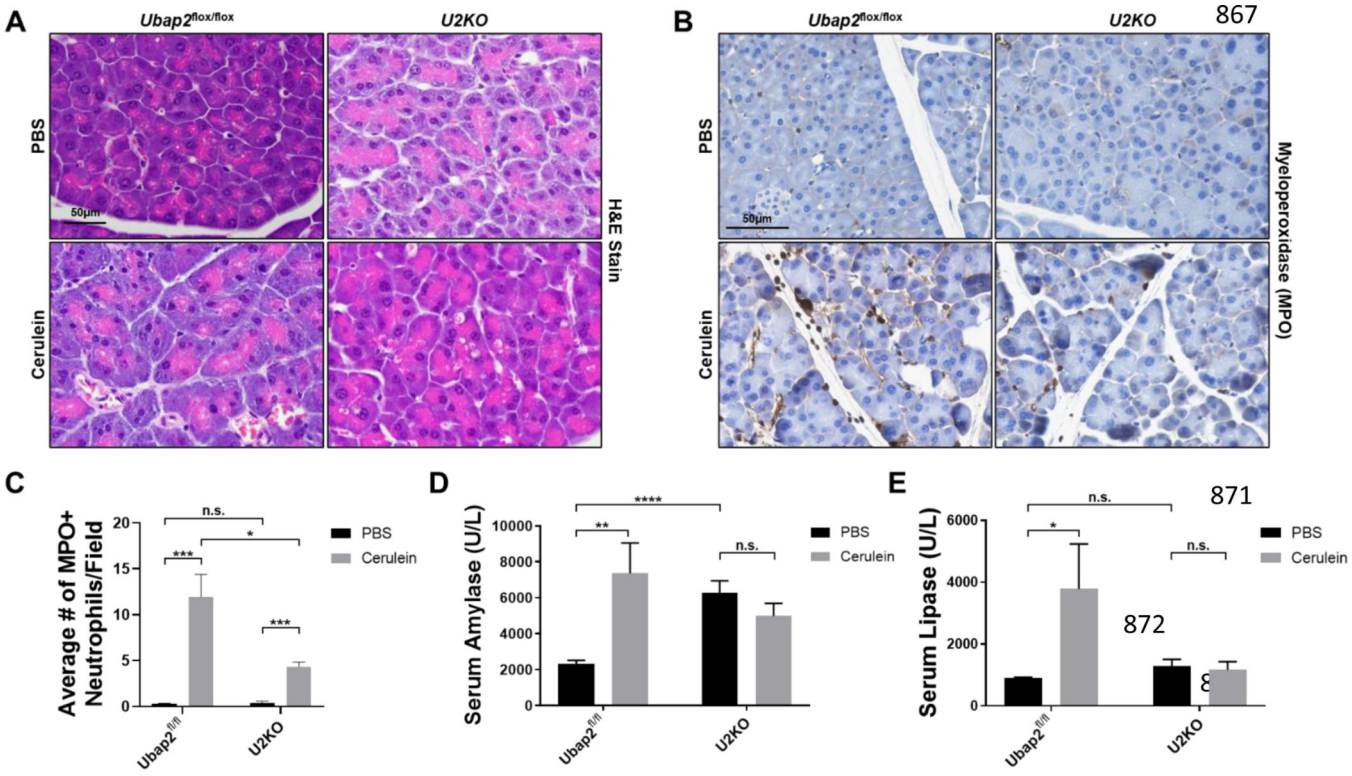

Figure 6. The Cerulein-induced pancreatitis response in *Ubap2*$^{flox/flox}$ and *U2KO* mice.

(A) H&E Staining of pancreatic tissue sections in Ubap2$^{flox/flox}$ and U2KO animals that were either injected with Cerulein (50ug/kg) or an equivalent volume of PBS as a control. **(B)** Histological Stains ofMyeloperoxidase in tissues of control animals and U2KO animals under either PBS or cerulean treatment and its quantification **(C).** (**D**-**E**) Serum Amylase **(D)** and lipase **(E)** levels of control (*Ubap2*$^{flox/flox}$) and U2KO animals measured in U/L. Baseline reference ranges: AMYL = 1691–3615U/L,LIPA = 600–1000U/L. Comparisons were made with the Student's T-test. Data are expressed as mean ± standard error of the mean (SEM), n=5–7. All analyses were performed through GraphPad-PRISM (7.04) (N.S. = Not significant).

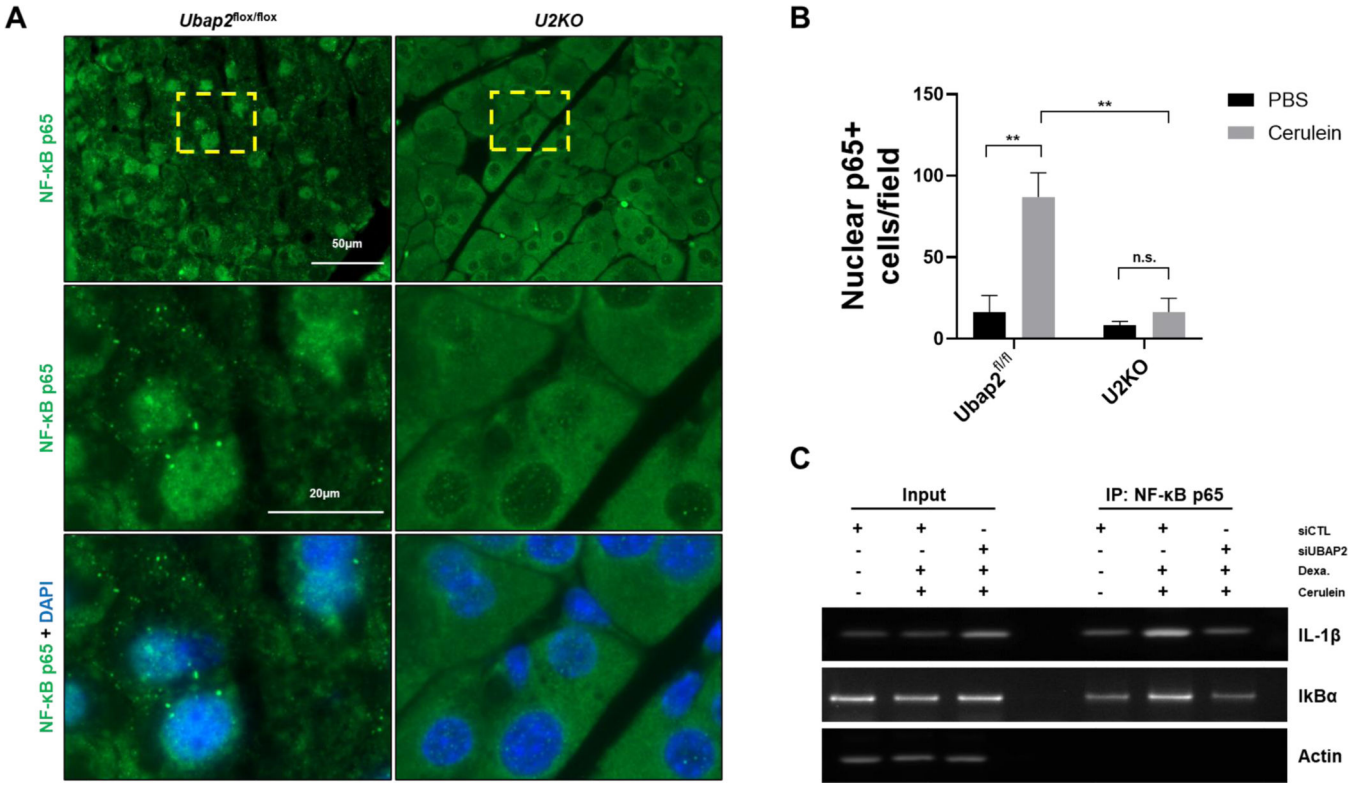

Figure 7. NF-κB signaling is reduced in *U2KO* mice when challenged with cerulein.

(A) NF-κB immunofluorescence staining in U2KO mice and control animals. Pancreatic tissue was taken from animals after Cerulein (50ug/kg) or an equivalent volume of PBS as a control (Figure S2B). Nuclei are stained with DAPI (blue). **(B)** Quantification of 40X magnification images from U2KO animals or control animals. Graph was generated from the number of positive cells within a single image field of a slide. 8 images are taken per animal and 4 animals were used per group analyzed. (**C**) Chromatin immunoprecipitation assays in AR42J cells were after 150nM cerulein for 24 hours or an equivalent volume of PBS. Cells were transiently transfected with either a nontargeting scramble siRNA or an siRNA targeting Ubap2. DNA gels were run from PCR-amplified products targeting the IL-1β promoter or the IκBα promoter region. Actin is used as a control for DNA loading. Comparisons were made with the Student's T-test. Data are expressed as mean ± standard error of the mean (SEM), n=5–7. All analyses were performed through GraphPad-PRISM (7.04) (N.S. = Not significant).